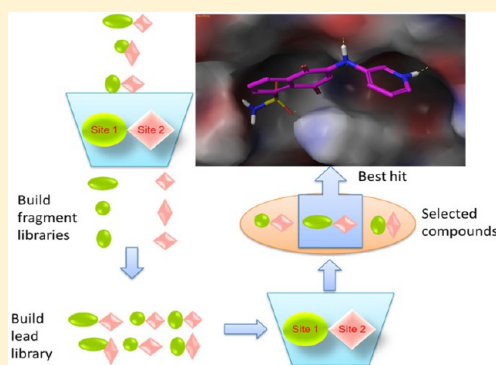


## Discovery of Novel STAT3 Small Molecule Inhibitors via in Silico Site-Directed Fragment-Based Drug Design

Wenying Yu,<sup>†</sup> Hui Xiao,<sup>‡</sup> Jiayuh Lin,<sup>‡</sup> and Chenglong Li<sup>\*,†</sup><sup>†</sup>Division of Medicinal Chemistry and Pharmacognosy, College of Pharmacy, The Ohio State University, Columbus, Ohio 43210, United States<sup>‡</sup>Center for Childhood Cancer, The Research Institute at Nationwide Children's Hospital, Department of Pediatrics, College of Medicine, The Ohio State University, Columbus, Ohio 43205, United States

## S Supporting Information

**ABSTRACT:** Constitutive activation of signal transducer and activator of transcription 3 (STAT3) has been validated as an attractive therapeutic target for cancer therapy. To stop both STAT3 activation and dimerization, a viable strategy is to design inhibitors blocking its SH2 domain phosphotyrosine binding site that is responsible for both actions. A new fragment-based drug design (FBDD) strategy, in silico site-directed FBDD, was applied in this study. A designed novel compound, 5,8-dioxo-6-(pyridin-3-ylamino)-5,8-dihydronaphthalene-1-sulfonamide (LY5), was confirmed to bind to STAT3 SH2 by fluorescence polarization assay. In addition, four out of the five chosen compounds have IC<sub>50</sub> values lower than 5  $\mu$ M for the U2OS cancer cells. 8 (LY5) has an IC<sub>50</sub> range in 0.5–1.4  $\mu$ M in various cancer cell lines. 8 also suppresses tumor growth in an in vivo mouse model. This study has demonstrated the utility of this approach and could be used to other drug targets in general.



## ■ INTRODUCTION

Constitutive activation of STAT3 has been found in a wide variety of cancers, including breast cancer, sarcomas, and other cancers, promoting it as a very attractive therapeutic target. Cytokines, hormones, and growth factors binding to the cell surface receptors can activate the JAK-STAT signaling pathway. Activated receptors activate JAK kinase(s) and autophosphorylate themselves. Subsequently, the STAT3 monomer is activated through phosphorylation at its tyrosine705 (pTyr705) by the same kinases through STAT3 SH2 domain binding to pTyr loop of the activated receptors, leading to STAT3 homodimer formation through its SH2 domain dimerization. The dimerized STAT3 then translocates into the nucleus and binds to DNA, turning on a host of oncogenes. Altogether, these events lead to cell proliferation, apoptosis resistance, etc. To block both phosphorylation and dimerization processes, STAT3 inhibitors should compete with the native phosphotyrosine (pTyr705) loop by binding to the STAT3 SH2 domain (Figure 1).

Several series of STAT3 dimerization inhibitors have been discovered via both computational and experimental methods. (1) Phosphopeptide mimics were initially developed as STAT3 inhibitors to compete with the native phosphopeptide of the STAT3 protein. For example, PM-73G is a phosphopeptide mimic STAT3 inhibitor that can completely inhibit STAT3 Tyr705 phosphorylation at 0.5–1  $\mu$ M level in various cancer cell lines.<sup>1</sup> Another phosphopeptide mimic, pCinn-Leu-cis-3,4-methanoPro-Gln-NHBn, has the lowest reported IC<sub>50</sub> value at

69 nM, as determined by the fluorescence polarization method.<sup>2</sup> (2) Peptidomimetics were also designed to target the STAT3 SH2 domain. Peptidomimetics are derived from phosphopeptides that mimic peptides but do not necessarily contain phosphate groups. For example, XZH-5 was designed using a structure-based approach to inhibit the formation of STAT3 dimers.<sup>3,4</sup> (3) Various small molecules have been reported to inhibit STAT3 dimerization, making them more druggable candidates. STA-21 discovered by structure-based virtual screening was one of the first reported small inhibitors. It inhibits STAT3 dimerization, DNA binding, and STAT3-dependent luciferase reporter activity in breast cancer cells.<sup>5</sup> Another small molecule, Stattic, was discovered by high-throughput screening and has been shown to selectively inhibit activation, dimerization, nuclear translocation of STAT3, and to increase apoptosis in STAT3-dependent cancer cell lines.<sup>6</sup> Among all the reported nonpeptidomimetic small inhibitors, 5-hydroxy-9,10-dioxo-9,10-dihydroanthracene-1-sulfonamide (LLL12) has the lowest IC<sub>50</sub> (0.16–3.09  $\mu$ M<sup>7</sup>), inhibiting STAT3 phosphorylation and the growth of human cancer cells. However, so far, there has been no STAT3-targeting drug approved by the FDA. The search for more druggable STAT3 inhibitors with high potency and excellent bioavailability remains extremely important.

Received: January 17, 2013

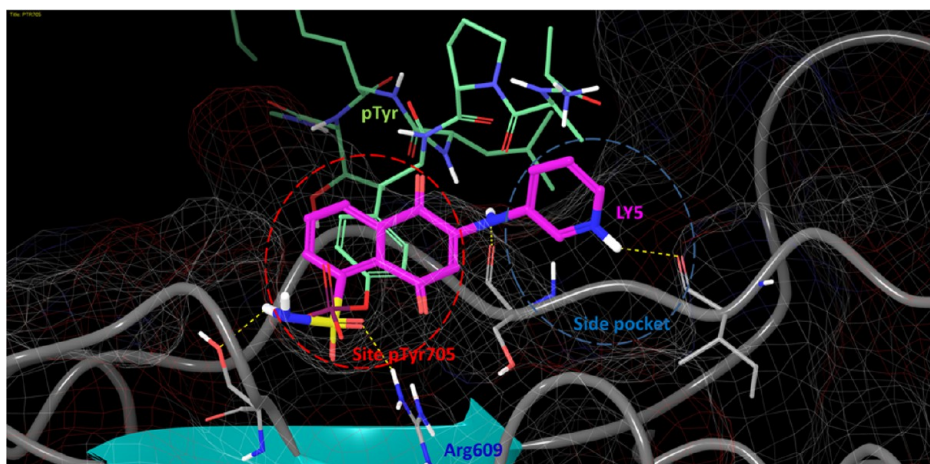


**Figure 1.** Docking model of STAT3 inhibitor **8** binding to the STAT3 SH2 domain (PDB 1BG1), generated by AutoDock4 and viewed by Maestro. The two key binding pockets are called “site pTyr705” (red circle) and “side pocket” (blue circle). Carbon atoms of **8** are colored purple, and those of the pTyr peptide are colored green. The style of molecular surface is mesh, colored according to element property.

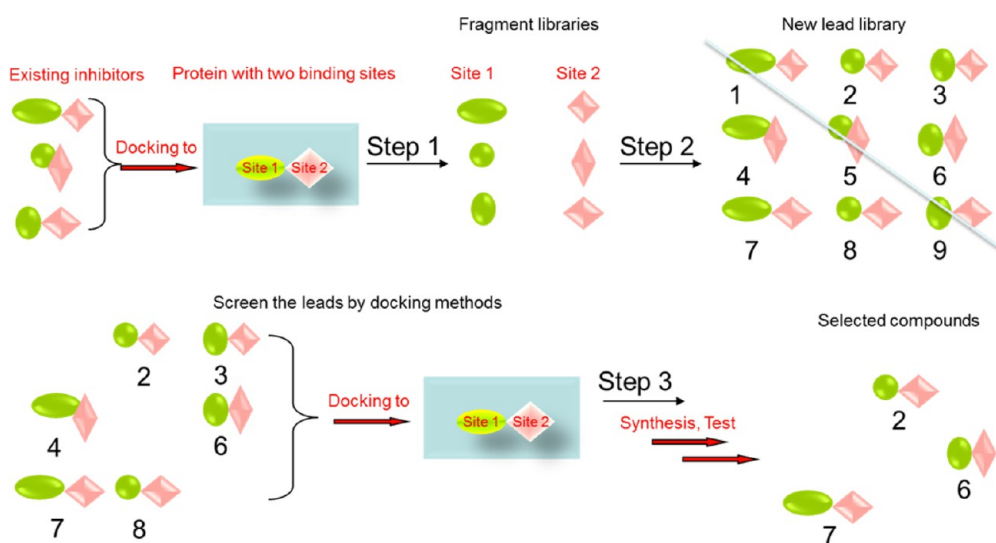


**Figure 2.** Site-directed FBDD strategy. Step 1: Fragment libraries are categorized from existing inhibitors according to their binding modes. Step 2: New lead library is merged from randomly selected fragments from site-specific fragment sublibraries. (Any existing inhibitors are removed from the new lead library.) Leads are selected after evaluating docking modes to the target. Step 3: Final hits are identified after synthesis and testing.

**Table 1.** Comparison of Conventional FBDD and in Silico Site-Directed FBDD

	Conventional FBDD	<i>In silico</i> site-directed FBDD
<b>Fragments library</b>	Screened by X-ray, NMR and other methods	Built from known inhibitors and divided into binding site specific sub-libraries according to docking poses
<b>Linkers</b>	Selected from linker libraries or from chemical intuition	Original linkers or bioisosters derived from original linkers
<b>Merge methods</b>	Fragments are randomly merged together	Fragments selected from sub-libraries are merged together
<b>Pre-selected candidates</b>	According to structural variety, purchase/synthesis availability or chemical intuition	According to computational docking results

Fragment-based drug design (FBDD) has emerged as a new strategy for drug discovery in the past decade. FBDD as a design-intensive method complements the resource-intensive conventional drug discovery methods such as high-throughput screening and combinatorial chemistry.<sup>8</sup> Conventional FBDD

has made some improvements on efficiency and cost-effectiveness in drug design, and several drug candidates designed by this methodology are currently under clinical trials. Computational fragment-based drug design is another FBDD approach. For example, Chen and Shoichet utilized the



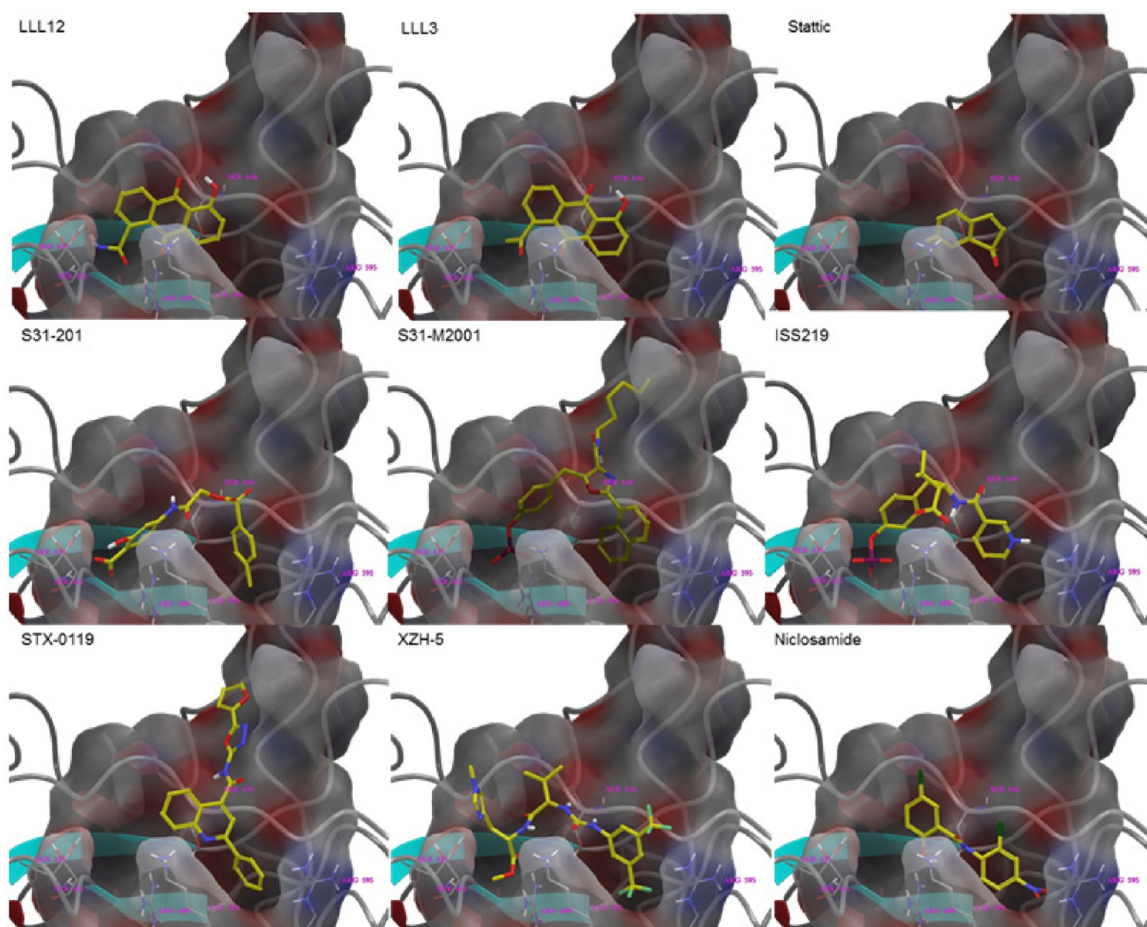


**Figure 3.** Docking modes of the selected known STAT3 inhibitors with the STAT3 SH2 domain (PDB 1BG1), generated by AutoDock4. Surface representation was created with Maestro.

computational fragment-based approach and successfully discovered potent *de novo* inhibitors against CTX-M, while the docking screens of lead-like compound libraries failed to identify any lead-like inhibitors.<sup>9</sup>

In this article, we present the concept of *in silico* site-directed FBDD as a computational FBDD approach, summarized in Figure 2.

With our *in silico* approach, fragment libraries are built from known inhibitors and are divided into binding site specific sublibraries according to docking poses. Linkers from the known inhibitors are the first choices to join fragments, however, new linkers based on the concept of bioisosterism<sup>10</sup> may also be applied to join fragments. New linkers designed in this fashion can often maintain the original binding interactions or even enhance binding. With merging, the joining of fragments and linkers is different in our computational approach compared to conventional FBDD. Conventional approaches randomly merge fragments together while our presorted, site-specific fragment sublibraries are recombined to maximize the possibility of obtaining novel compounds with potentially better druggability (e.g., potency, selectivity, ADME/Tox properties, and synthetic ease, etc). Merged potential candidates may be quickly screened via computational docking methods to further narrow the number of molecules that will be selected for synthesis and testing. The comparisons between conventional and *in silico* site-directed FBDD methods are summarized in Table 1.

To test the method, we have applied the approach to the case of STAT3 inhibitor design. The STAT3 fragment library was generated from nine known inhibitors with proven affinity and established pharmacological activities for STAT3. New leads were designed to target site pTyr705 and the side pocket (Figure 1). The STAT3 fragment library was divided into two specific sublibraries for the site pTyr705 and the side pocket based on the docking poses of the inhibitors to the crystal structure of STAT3 SH2 domain (PDB 1BG1).

To efficiently evolve the fragments into leads, several considerations were made when choosing the linker and performing the merging. A desirable linker should allow sufficient flexibility for the fragments to maintain their poses in the binding sites and enhance binding affinity and/or biophysical features such as water solubility. Most importantly, the chosen linker should not complicate synthesis. In this case, a secondary amine was chosen as the linker. The merged candidates were then screened via computational docking, and the compounds with the most favorable docking energies and well-clustered binding poses were selected for synthesis and experimental testing. This led to a new class of STAT3 inhibitors.

## RESULTS

**Design. Step 1: Fragment Libraries Were Categorized from the Known STAT3 Dimerization Inhibitors Based on Their Binding Modes.** To build fragment libraries from the

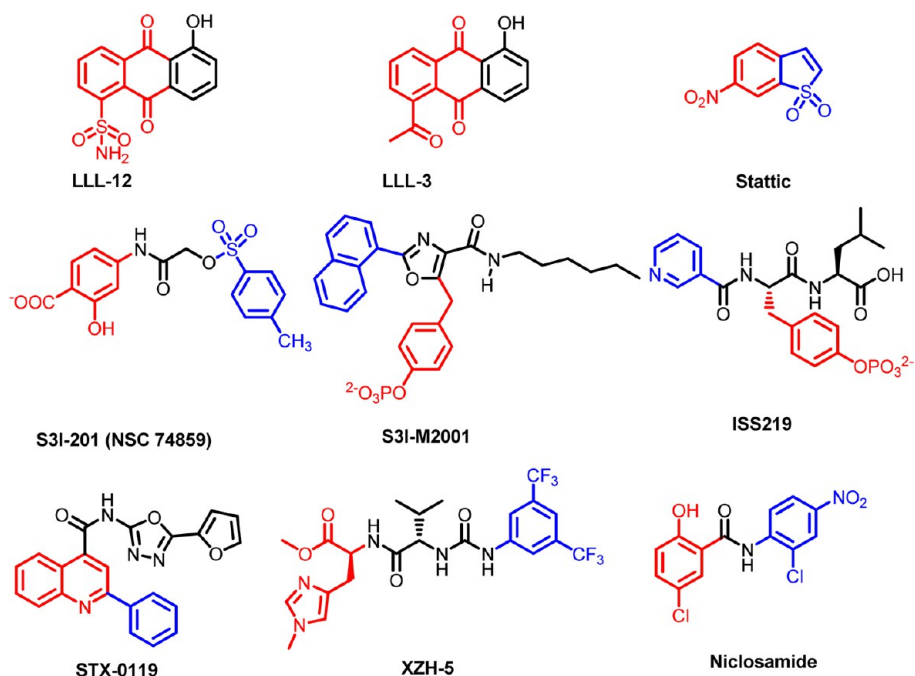


**Figure 4.** Chemical structures of the selected STAT3 dimerization inhibitors. According to the docking modes in Figure 3, the fragments binding to the pTyr705 site are colored red and those binding to the side pocket are colored blue.

known STAT3 inhibitors,<sup>3,5-7,11-15</sup> the compounds were docked to the STAT3 SH2 domain (PDB 1BG1). The initial docking results are shown in Figure 3. On the basis of the binding modes, the fragments were divided into libraries specific for each of the two binding sites: site pTyr705 and side pocket (Figures 4 and 5).

**Step 2: New lead Library Was Built by Linking Selected Fragments from Different Fragment Sublibraries.** On the basis of the docking modes for known STAT3 inhibitors,

naphthalene-5,8-dione-1-sulfonamide (**1**) exhibited the most interactions with site pTyr705 by forming two hydrogen bonds with Arg609 and an additional hydrogen bond with Ser613. Additionally, as part of **13** (LLL12), one of the most potent small nonpeptidomimetic inhibitors of STAT3 dimerization, **1** is an attractive starting point for the synthesis of new STAT3 inhibitors. Therefore, **1** was selected as the component targeting site pTyr705 and was randomly linked to fragments from the side pocket sublibrary to form new potential inhibitors.

The linker was designed based on the rationale described previously, that the new linker could maintain or even enhance the binding affinity of the two fragments and that the synthetic strategy would be feasible. On the basis of the docking mode of **13** in Figure 3, the phenol ring of LLL12 is the original linker of **1**. Given the difficulty of synthesis, the original linker was simplified into an isopropyl group, which was subsequently evolved into an isopropyl amine group based on bioisosterism. To further reduce the synthetic difficulty, the isopropyl amine was modified to a dimethyl amine linker as shown in Figure 6.

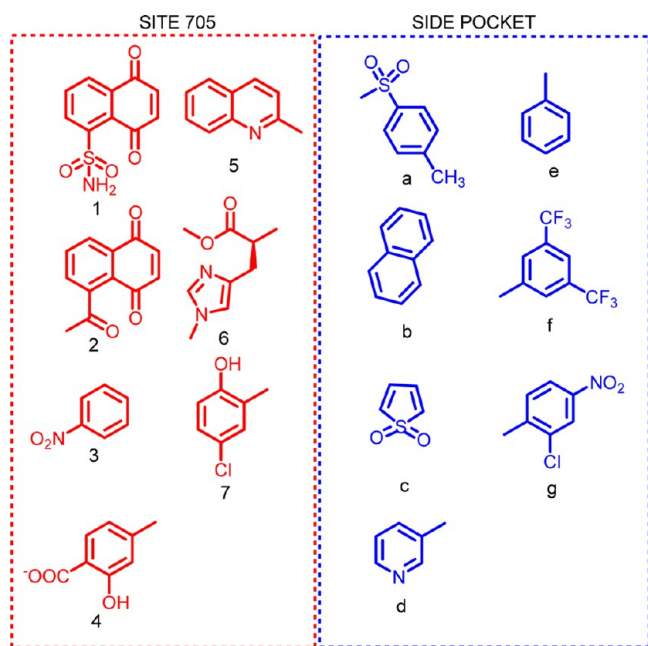


**Figure 5.** Categorized fragment sublibraries, site pTyr705 (1–7) and side pocket (a–g) (the fragment phosphotyrosine group was not included in the fragment libraries due to its peptidomimetic property).

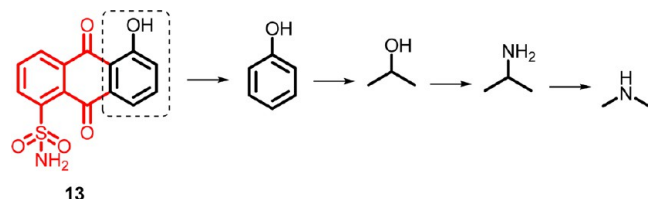


**Figure 6.** The evolution of linker design.

Finally, the dimethyl amine group was selected as a suitable linker after docking results indicated that candidates with this linker could form hydrogen bonds with the backbone of Ser636 in a similar fashion as the hydroxyl group of **13** (Figure 7).

**Step 3: Final Leads for Further Synthesis and Tests Were Selected by Repositioning the Compounds from Lead**

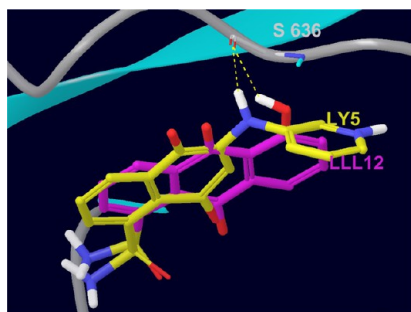


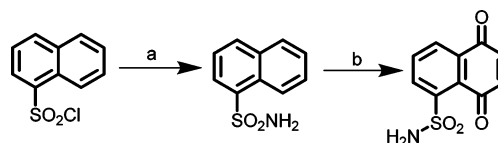
**Figure 7.** The docking modes of **13** (LLL12) and **8** (LY5). Both linkers, the hydroxyl group in **13** and secondary amine group in **8**, form hydrogen bonds with the Ser636.

**Library to STAT3 SH2 domain.** Docking the new lead library to the STAT3 SH2 domain, compounds were ranked based on the docking scores and clustering, and compounds that could not reposition to the binding pockets were removed from consideration. The compounds that were ultimately selected for synthesis and testing are shown in Table 2.

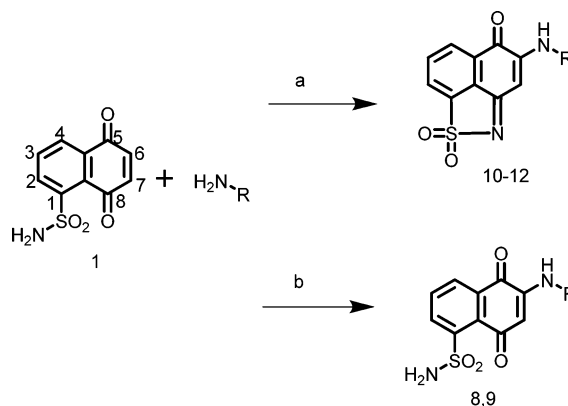
**Chemistry. Synthesis of Fragment 1.** **1** was synthesized as previously described<sup>7</sup> with some modifications; procedures are shown in Scheme 1. Naphthalenesulfonylchloride reacted with ammonium hydroxide at room temperature and precipitated white crystal naphthalenesulfonamide with high purity ready for next step synthesis and 90.2% yield. Naphthalenesulfonamide was oxidized by chromium trioxide in an acidic environment. This reaction is highly time sensitive because the longer reaction times result in more byproducts. To achieve the optimal reaction time, the solvent can be preheated to reflux, and then chromium trioxide added into the reaction system. **1** was not very stable during the column separation, so flash column was used for purification.

**Synthesis of Novel STAT3 Inhibitors.** Fragment **1** and aromatic amines were catalyzed by Cu(OAc)<sub>2</sub>·H<sub>2</sub>O in an acidic environment (Scheme 2). Reaction system was heated to reflux

**Scheme 1. Preparation of Fragment 1**



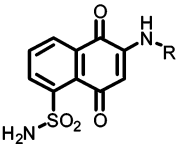
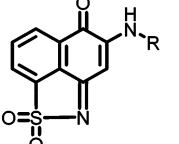
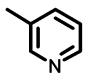
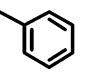
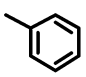
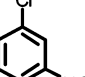
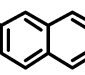
**Scheme 2. Synthesis of Designed Inhibitors by Regioselective Coupling Two Fragments Together (R Group Is Described in Table 2 for Each Product)<sup>a</sup>**



<sup>a</sup>Reagents and conditions: (a) Cu(OAc)<sub>2</sub>·H<sub>2</sub>O, AcOH; (b) Cu(OAc)<sub>2</sub>·H<sub>2</sub>O, AcOH and H<sub>2</sub>O (1:10 v/v).

and terminated when **1** was consumed completely. This reaction is a novel regioselective method which can selectively react to position 6 of fragment **1**. No regioisomers at position 7 were detected in the byproducts. The atom numbering of **1** is shown in Scheme 2. The purification of STAT3 inhibitors is also very interesting. As the bands of novel STAT3 inhibitors were red or brown, the elution of products was quickly monitored based on the visible bands. As reported in other naphthoquinone coupling reactions, solvent has a large effect

**Table 2. Chemical Structures, Docking Scores, and IC<sub>50</sub> of the Designed STAT3 Inhibitors**

							
Compound	R	Docking score <sup>a</sup> (kcal/mol)	IC <sub>50</sub> <sup>b</sup> (μM)	Compound	R	Docking score (kcal/mol)	IC <sub>50</sub> (μM)
<b>8</b>		-7.3	0.5	<b>10</b>		-7.1	5.0
<b>9</b>		-7.2	>5.0	<b>11</b>		-8.4	1.4
				<b>12</b>		-8.0	2.5

<sup>a</sup>Docking scores were calculated by AutoDock4. <sup>b</sup>IC<sub>50</sub> was tested on sarcoma cell line U2OS.



on the yield. Glacial acetic acid was the best choice for our reaction. If water is added to the reaction, the yield will decrease. However, if glacial acetic acid is the only solvent, the major product will be cyclized compounds because the sulfonamide group can attack the nearby 1-ketone and deplete a water molecule to form the cyclized products such as **10**, **11**, and **12**. To keep the free sulfonamide group to maintain the best docking pose, we had to use a mixed solvent system by adding water to glacial acetic acid in a volume ratio 1:10. This decreased the yield by approximate 20%.

**Biological and Biochemical Assays. Cell Viability Assay.** Initially, IC<sub>50</sub> values for all of the compounds were tested with U2OS cell line. Then two most potent compounds, **8** (LY5) and **11**, were further tested together with **13** in two other RD2 and RH30 cell lines. As **13** had the lowest IC<sub>50</sub> among the known small inhibitors, it was selected as a control compound. The results showed that **8** had lower IC<sub>50</sub> than **13** in cell lines RD2 and U2OS and similar IC<sub>50</sub> to **13** in cell line RH30. **11** had a comparable IC<sub>50</sub> as **13** in cell lines RD2 and U2OS (Table 3).

**Table 3. IC<sub>50</sub> Values for Human Sarcoma Cells (RD2, RH30, and U2OS) Inhibition by STAT3 Inhibitors, **13** (LLL12), **8**, and **11****

compd	IC <sub>50</sub> values (μM) vs cell lines		
	U2OS	RH30	RD2
<b>13</b>	1.00	0.47	2.85
<b>8</b>	0.52	0.55	1.39
<b>11</b>	1.39	1.14	2.56

**Compound **8** Inhibits STAT3 Phosphorylation and Induces Apoptosis in Human Sarcoma Cancer Cells.** To examine the inhibition of STAT3 phosphorylation, Western blot assays were performed to detect the abundance of phosphorylated STAT3 (P-STAT3) after RH30 cells were treated with **11** (0.5–2.5 μM) or **8** (0.25–1 μM) for 16 h. STAT3 phosphorylation was reduced in a dose-dependent manner, with **8** and **11** almost completely inhibiting Tyr705 phosphorylation at 0.5 and 1 μM, respectively (Figure 8). Since **8** was shown to be a more potent inhibitor of STAT3 phosphorylation than **11** in the RH30 cell line, it was further tested in EW8 sarcoma cells. Western blots of EW8 cells treated with **8** (0.5–1.0 μM) for 8 h again reveals a dose-dependent decrease in formation of P-STAT3 (Figure 9). The expression of total STAT3 was not changed in both RH30 and EW8 cell lines, indicating that the decrease of P-STAT3 was not due to a constitutional decrease of total STAT3 expression. **8** was not found to inhibit phosphorylation

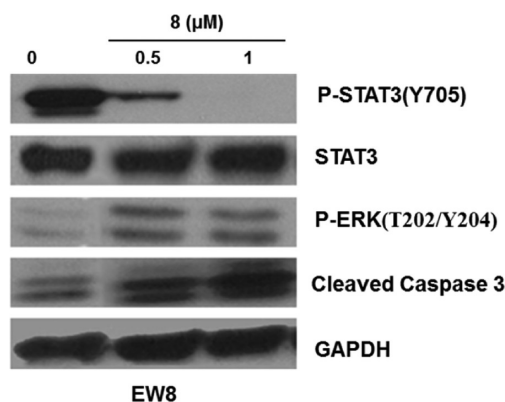


**Figure 9.** Compound **8** inhibits constitutive STAT3 phosphorylation. Ewing's sarcoma cell line EW8 was treated with **8** (0.5–1 μM) for 8 h, then whole-cell extracts were prepared and phospho-STAT3 was detected by Western blot assay, revealing a decrease in STAT3 phosphorylation.

of the kinase ERK1/2. The inhibition of STAT3 phosphorylation by **8** seems to be consistent with the induction of apoptosis, as evidenced by the presence of cleaved caspase 3 (Figure 9).

**Compound **8** Inhibits STAT3 Phosphorylation Induced by IL-6.** IL-6 can induce the activation of STAT3.<sup>16</sup> The MCF-7 breast cancer cell line was used to determine the ability of **8** to inhibit IL-6 induced STAT3 phosphorylation because MCF-7 cells do not express persistently phosphorylated STAT3. In control experiments, IL-6 elevated STAT3 phosphorylation in MCF-7 cells, while **8** and **11** blocked the stimulation, with phosphorylated STAT3 abrogated at low concentrations (Figure 10). The DAOY medulloblastoma cancer cell line was used to further determine the ability of **8** to inhibit IL-6 induced STAT3 phosphorylation. In control experiments, IL-6 elevated STAT3 phosphorylation in DAOY cells, while **8** blocked the stimulation, with phosphorylated STAT3 abrogated at low concentrations (Figure 11).

**Compound **8** Does Not Inhibit STAT1 Phosphorylation Induced by IFN-γ.** IFN-γ can induce the activation of STAT1<sup>17</sup> that acts as a tumor suppressor in certain occasions. The selectivity of **8** for STAT3 inhibition was evident when compared with that for STAT1. IFN-γ treatment elevated STAT1 phosphorylation in DAOY cells, whereas **8** pretreatment had no effect on the extent of STAT1 phosphorylation (Figure 12).

**Compound **8** Suppresses Tumor Growth of Breast Cancer in a Mouse Tumor Model.** We performed in vivo studies to

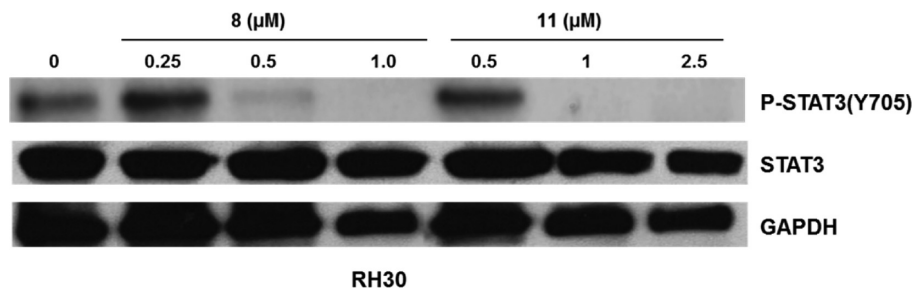


**Figure 8.** **11** and **8** inhibit constitutive STAT3 phosphorylation. Human rhabdomyosarcoma cell line RH30 was treated with **11** (0.5–2.5 μM) and **8** (0.25–1 μM) for 16 h, then whole-cell extracts were prepared and phospho-STAT3 was detected by Western blot assay, revealing a decrease in STAT3 phosphorylation.

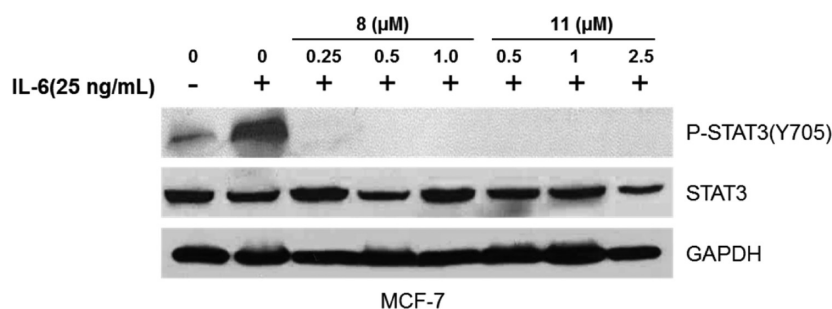


**Figure 10.** 11 and 8 inhibit IL-6 induced STAT3 phosphorylation in MCF-7 breast cancer cells. The MCF-7 cells were serum-starved overnight, then left untreated or treated with 11 (0.5–2.5 μM) or 8 (0.25–1 μM) for 5 h, followed by stimulation by IL-6 (25 ng/mL). The cells were harvested at 30 min and analyzed by Western blot assays.

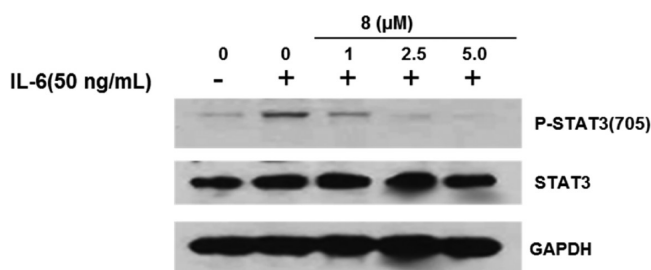


**Figure 11.** 8 inhibits IL-6 induced STAT3 phosphorylation in DAOY cancer cells. The DAOY cells were serum-starved overnight, then left untreated or treated with 8 (1–5 μM) for 2 h, followed by stimulation by IL-6 (50 ng/mL). The cells were harvested at 30 min and analyzed by Western blot assays.

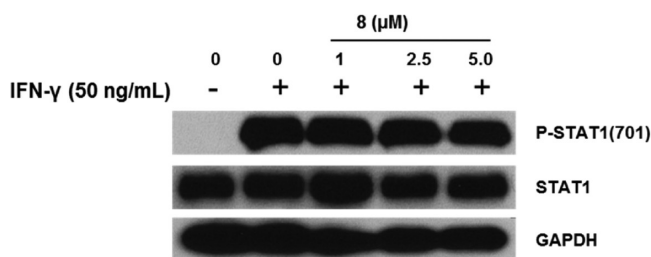


**Figure 12.** IFN-γ induced STAT1 phosphorylation in DAOY cancer cells. The DAOY cells were serum-starved overnight, then left untreated or treated with 8 (1–5 μM) for 2 h, followed by stimulation by IFN-γ (50 ng/mL). The cells were harvested at 30 min and analyzed by Western blot assays. The results show that 8 did not inhibit STAT1 phosphorylation.

confirm the tumor suppression efficacy of 8 and its potential usage for breast cancer treatment. MDA-MB-231 cells were injected subcutaneously into nude mice for the induction of xenografts. After a 21 days of treatment, the morphological data showed that 8 suppressed xenograft growth and significantly ( $P < 0.001$ ) shrank the tumor sizes (Figure 13).

**Fluorescence Polarization (FP) Assay.** FP assay was used to further prove the binding of 8 to the STAT3 SH2 domain. Screening was performed at physiologically relevant temperature 37 °C. Before each experiment, 8 was prepared freshly from the stock solution. Compound 8 increased its background fluorescence reading at 595 nm at high concentrations, so the control solutions for each concentration were prepared by mixing buffer, 8, and fluorescence-labeled peptides together. Inhibition curves were fitted in Sigmaplot11.0 (Figure 14), and  $K_i$  value is 2.5 μM using a mathematical model developed for FP assay. So the experimental  $\Delta G$  value of 8 is  $-7.9$  kcal/mol,

which is comparable to the AutoDock4 computed  $\Delta G$  value of  $-7.3$  kcal/mol.

## DISCUSSION

Even though there have been numerous attempts on drug design using computational fragment-based approach and molecular hybridization, in this work, we introduce a new approach that combines target-structure-based in silico docking, site-directed fragment hybridization, and bioisosterism to recombine fragments of known inhibitors to form new lead molecules. The successful application of this method is detailed in the design of a novel STAT3 inhibitor scaffold, leading to compounds with low  $IC_{50}$  values and strong binding affinity to STAT3 SH2 domain. This study has several significant findings: (1) The use of fragment sublibraries based on the docking modes of known inhibitors was an efficient method to design potential new inhibitors. This method is potentially more reliable than virtual screening of fragment libraries and less costly than conventional methods like high-throughput screening. It is also distinct from the molecular hybridization,<sup>18</sup> as in our approach, fragments are linked together based on structural information of a specific target and the linked new compound is designed to bind to the same target. In addition, the final docking step of the merged fragments acts as an extra filter to ensure that key interactions are maintained or even optimized prior to synthesis. (2) The secondary amine linker used in the design is a bioisostere of the hydroxyl group in 13 that can maintain both the binding poses of the fragments and the binding affinity. (3) The synthesis of novel STAT3 inhibitors presents a new highly regioselective coupling method. The major product is connected at position 6 of the naphthoquinone. Compared to 13, the novel series of STAT3 inhibitors are superior, with lower synthetic cost and larger space for further modification. 13 has some disadvantages such as the need for the expensive synthetic material 3-hydroxy-2-pyrone, time-consuming purification to separate the regioisomers, and difficulty in modifying the three-ring system. The novel STAT3 inhibitors can overcome these shortcomings. The synthetic materials for novel STAT3 inhibitors are about 10 times less costly, the reaction has much higher selectivity to react to 6-naphthalene-5,8-dione-1-sulfonamide than to 7-naphthalene-5,8-dione-1-sulfonamide, and it is very easy to modify the novel STAT3 inhibitors to fit the side pocket by alternating the amine reagents. (4) The fluorescence polarization (FP) assay proved that 8 binds to STAT3 SH2 domain with a  $K_i$  value of 2.5 μM. (5) For in vitro study, the  $IC_{50}$  of 8 is superior to that of 13 in two different cancer cell lines, U2OS and RD2, while 13 has the lowest  $IC_{50}$  among all the reported

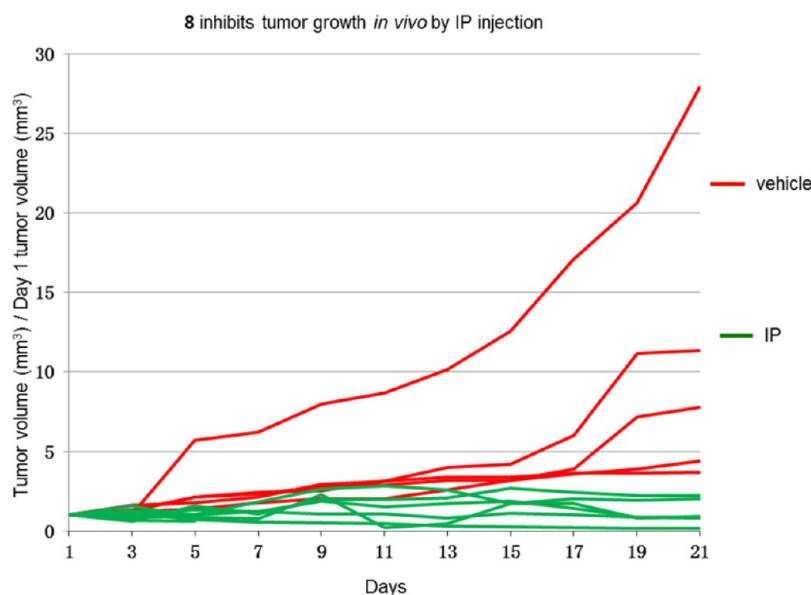


**Figure 13.** Compound **8** suppresses tumor growth of MDA-MB-231 breast cancer cells in mouse tumor model *in vivo*. Tumor growth was determined by measuring length ( $L$ ) and width ( $W$ ) of the tumor every other day with a caliper. The tumor volume was calculated according to the formula: tumor volume =  $0.5236 \times L \times W^2$ . The treatment lasted for 21 days. The results showed that **8** significantly suppresses the tumor growth ( $P < 0.001$ ).

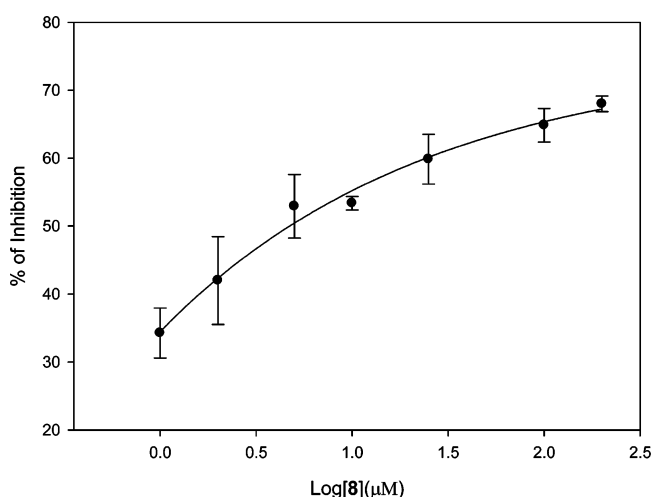


**Figure 14.** Compound **8** binds to STAT3 SH2 domain. Inhibition of binding of fluorescein-labeled phosphopeptides to the SH2 domains of STAT3 by **8** at 37 °C was assayed by fluorescence polarization. Error bars represent standard deviation.

nonpeptidomimetic small molecule inhibitors targeting SH2 domain previously. (6) For DAOY cell line, **8** reveals a clear selectivity between IL-6 induced P-STAT3 and IFN- $\gamma$  induced P-STAT1, as shown in Figure 11 and 12. 7) For *in vivo* study, **8** also significantly suppresses tumor growth of breast cancer cells in a mouse tumor model.

This method has the potential to be efficient in new lead generation, but it requires a few known inhibitors for certain targets. For targets with many known inhibitors, such as kinases, *in silico* site-directed FBDD would likely be useful and produce many new leads. However, this drug design method could also be used for a target without known inhibitors, if its homologous targets exist with sufficient known inhibitors. Fragment libraries built from these inhibitors still could be used to search for new inhibitors for the target protein. An additional

shortcoming is that ligand efficiency (LE) is unlikely to increase significantly during the fragment recombination unless the binding modes of fragments can be greatly improved without increasing their sizes. One might not expect deconstruction of a potent lead to always derive high quality fragments if the synergy between two nonadjacent binding interactions is lost during the fragmentation. How reliably fragments can be recombined to maintain synergy will need to be further examined. In this work, potency does not improve a lot but the new compound is better in several other aspects as described above. In this sense, this approach is a useful option for certain design purposes, be it on synthetic easiness, potency or selectivity improvement, necessary drug property (ADMT/Tox) alteration to move the compound forward in the drug design pipeline, etc.

## CONCLUSIONS

Recombination of two fragments from existing STAT3 activation and dimerization inhibitors through *in silico* site-directed FBDD is an efficient and feasible method to design novel potent STAT3 inhibitors. Linker selection was explored so that the synthetic strategy was feasible, the designed binding modes of the fragments were preserved, and the new linker itself enhanced the binding affinity of the fragments. Four out of five synthesized compounds have  $IC_{50}$  lower than 5  $\mu M$  for cancer cell line U2OS. The lead compound **8** has an  $IC_{50}$  between 0.5 and 1.4  $\mu M$  in various cancer cell lines. The fluorescence polarization (FP) assay validated the binding of **8** to STAT3 SH2 domain. The experimental  $\Delta G$  value of **8** is  $-7.9$  kcal/mol, which is comparable to the AutoDock4 computed  $\Delta G$  value of  $-7.3$  kcal/mol. In addition, **8** has been demonstrated to significantly decrease STAT3 phosphorylation/activation, shows a clear inhibitory selectivity of P-STAT3 over P-STAT1, and significantly suppresses tumor growth *in vivo*. This *in silico* site-directed FBDD strategy could be used for small molecule design to other drug targets.



## ■ EXPERIMENTAL SECTION

**FBDD.** General procedure of docking. Computational docking program AutoDock4 was used to dock all the existing inhibitors and our designed small molecules to predict their binding modes and approximate binding free energies to the STAT3 SH2 dimerization site.<sup>19</sup> Compounds were docked using the Lamarckian Genetic Algorithm. The docking procedure involved the preparation of the ligand and macromolecule using the Schrodinger software.<sup>20,21</sup> AutoDockTools was used to assign Gasteiger charges to the ligands. AutoGrid maps were then precomputed for all atom types in the ligand set. After 10 million energy evaluations were completed, all the resulting conformations of the ligands in the binding pocket of the macromolecule were clustered into groups according to their conformations with a root-mean-square deviation threshold of 1.5 Å. The most significant low energy clusters were identified and binding energies were evaluated.

**Chemistry. Chemicals and Reagents.** The solvents and reagents used in the present study were purchased from commercial suppliers and were used as received. Thin layer chromatography was performed with fluorescent silica coated aluminum sheets. Silica gel was purchased from Sigma-Aldrich Chemical Co. (Milwaukee, WI). The purities of all tested compounds are higher than 95% by HPLC, which were performed by analytical HPLC. Analytical HPLC was carried out with a Gemini 5  $\mu$  C18 110A column (250 mm  $\times$  4.6 mm) supplied by Phenomenex Inc. CA, USA. Two different gradients [water (0.1% TFA)/acetonitrile (0.1% TFA) and water (0.1% TFA)/methanol (0.1% TFA)] were used at 1 mL/min flow rate (method: 100:0 to 0:100 over 20 min followed by 0:100 to 100:0 over 10 min). Melting points (mp) were determined on a Thomas–Hoover capillary melting point apparatus. Proton nuclear magnetic resonance spectra were obtained with a Bruker Avance 300 (300 MHz) spectrophotometer (Billerica, MA).

**Naphthalene-5,8-dione-1-sulfonamide (1).** Naphthalenesulfonylchloride (16.8 g, 74.3 mmol) was dissolved in acetone (100 mL) and was stirred at 0 °C for 5 min. Ammonium hydroxide (100 mL) was dropped into the above mixture and stirred at room temperature for 3 h. Precipitated white crystals were filtered then acetone was removed at reduced pressure. The residue was washed in ethylacetate (3  $\times$  10 mL), producing a white solid powder which was used without further purification, yielding naphthalenesulfonamide (15.9 g, 90.2%); mp (147–149 °C). Naphthalenesulfonamide (500 mg, 2.41 mmol) was dissolved in slowly warming glacial acetic acid (5.0 mL). The mixture was heated to 90 °C and chromium trioxide (1.08 g, 10.85 mmol), which was dissolved in a mixture of water and glacial acetic acid (1:1 v/v, 3 mL), was added to the mixture solution. The above solution was stirred under reflux for 18 min. The solution was cooled to 0 °C, and water (50 mL) was added and stirred overnight at room temperature. The precipitated yellow powder was filtered, and the remaining solution was extracted with ether (3  $\times$  100 mL). The organic layer was collected, dried, and removed at reduced pressure. The yellow powder was combined and purified with silica column chromatography ethyl acetate–hexane (2:3 v/v) to yield **1** (110 mg, 19.3%); mp (186–188 °C).

**General Experimental Procedure for Scheme 2.** Fragment **1** (237 mg, 1 mmol), amine (1.2 mmol) and Cu(OAc)<sub>2</sub>·H<sub>2</sub>O (20 mg, 0.1 mmol) were solubilized by gently warming in AcOH (5 mL), refluxing for about 3 h. As detected by TLC, after **1** had completely reacted, all the volatiles were removed under reduced pressure. The resulting crude product was dissolved in a minimal volume of CH<sub>2</sub>Cl<sub>2</sub> and applied to a column of silica gel. The column was eluted with CH<sub>2</sub>Cl<sub>2</sub> or other solvents as indicated in the description of each product. The solvent was removed under reduced pressure to give products (**10**–**12**). Alternatively, **1** (237 mg, 1 mmol), amine (1.2 mmol), and Cu(OAc)<sub>2</sub>·H<sub>2</sub>O (20 mg, 0.1 mmol) were solubilized by gently warming in AcOH and H<sub>2</sub>O (1:10 v/v, 5.5 mL), refluxing for about 3 h. Following the same procedures, **8**–**12** were synthesized.

**5,8-Dioxo-6-(pyridin-3-ylamino)-5,8-dihydronaphthalene-1-sulfonamide (8).** The reactant amine is 3-amine-pyridine (113 mg, 1.2 mmol). The product was purified by silica gel column chromatography

eluting with CH<sub>2</sub>Cl<sub>2</sub>/EtOAc (8:1 v/v), followed by CH<sub>2</sub>Cl<sub>2</sub>/EtOAc (2:1 v/v), then further purified by recrystallization. Bright-red crystals (89 mg, yield: 27%); mp (>260 °C). <sup>1</sup>H NMR (300 MHz, DMSO)  $\delta$  9.52 (s, 1H), 8.63 (s, 1H), 8.44 (d, *J* = 7.9 Hz, 2H), 8.35 (d, *J* = 7.5 Hz, 1H), 7.96 (t, *J* = 7.7 Hz, 1H), 7.84 (d, *J* = 7.7 Hz, 1H), 7.48 (s, 1H), 7.35 (s, 2H), 6.13 (s, 1H). HRMS (ESI) of C<sub>15</sub>H<sub>11</sub>N<sub>3</sub>O<sub>4</sub>SNa [M + Na]<sup>+</sup> calcd, 352.0362; found, 352.0358.

**5,8-Dioxo-6-(phenylamino)-5,8-dihydronaphthalene-1-sulfonamide (9).** The reactant amine is aniline (0.11 mL, 1.2 mmol). Then the product was purified by silica gel column chromatography eluting with CH<sub>2</sub>Cl<sub>2</sub>, followed by CH<sub>2</sub>Cl<sub>2</sub>/EtOAc (8:1 v/v). Red crystals (85 mg, yield: 26%); mp (>260 °C). <sup>1</sup>H NMR (300 MHz, DMSO)  $\delta$  9.46 (s, 1H), 8.48–8.31 (m, 2H), 7.95 (t, *J* = 6.9 Hz, 1H), 7.61–7.21 (m, 7H), 6.14 (s, 1H). HRMS (ESI) of C<sub>16</sub>H<sub>12</sub>N<sub>2</sub>O<sub>4</sub>SNa [M + Na]<sup>+</sup> calcd, 351.0415; found, 351.0423.

**5H-Naphth[1,8-cd]isothiazol-5-one, 1,1-dioxide, 6-(phenylamino) (10).** The reactant amine is aniline (0.11 mL, 1.2 mmol). The product was purified by silica gel column chromatography eluting with CH<sub>2</sub>Cl<sub>2</sub>, then further purified by recrystallization. Red crystals (143 mg, yield: 46%); mp (>260 °C). <sup>1</sup>H NMR (300 MHz, DMSO)  $\delta$  9.78 (s, 1H), 8.39 (d, *J* = 7.1 Hz, 1H), 8.04 (q, *J* = 7.3 Hz, 2H), 7.55–7.33 (m, 4H), 7.25 (t, *J* = 6.9 Hz, 1H), 6.14 (s, 1H). HRMS (ESI) of C<sub>16</sub>H<sub>10</sub>N<sub>2</sub>O<sub>3</sub>SNa [M + Na]<sup>+</sup> calcd, 333.0304; found, 333.0329.

**5H-Naphth[1,8-cd]isothiazol-5-one, 1,1-dioxide, 6-(1'-chloro-3'-nitro-2'-phenylamino) (11).** The reactant amine is 2-chloro-4-nitroaniline (206 mg, 1.2 mmol). The product was purified by silica gel column chromatography eluting with CH<sub>2</sub>Cl<sub>2</sub>, followed by a CH<sub>2</sub>Cl<sub>2</sub>/EtOAc (8:1 v/v), then further purified by recrystallization. Orange crystals (189 mg, yield: 48.6%); mp (>260 °C). <sup>1</sup>H NMR (300 MHz, DMSO)  $\delta$  10.19 (s, 1H), 8.51 (d, *J* = 2.0 Hz, 1H), 8.45–7.93 (m, 4H), 7.83 (d, *J* = 8.8 Hz, 1H), 6.15 (s, 1H). HRMS (ESI) of C<sub>16</sub>H<sub>8</sub>ClN<sub>3</sub>O<sub>5</sub>SNa [M + Na]<sup>+</sup> calcd, 411.9765; found, 411.9764.

**5H-Naphth[1,8-cd]isothiazol-5-one, 1,1-dioxide, 6-(naphthylamino) (12).** The reactant amine is 2-naphthylamine (172 mg, 1.2 mmol). The product was purified by silica gel column chromatography eluting with hexane/CH<sub>2</sub>Cl<sub>2</sub> (1:4 v/v), followed by CH<sub>2</sub>Cl<sub>2</sub>. Red crystals (170 mg, yield: 47.3%), then further purified by recrystallization; mp (>260 °C). <sup>1</sup>H NMR (300 MHz, DMSO)  $\delta$  10.00 (s, 1H), 8.44 (dd, *J* = 7.2, 1.3 Hz, 1H), 8.31–7.86 (m, 7H), 7.78–7.30 (m, 4H), 6.33 (s, 1H). HRMS (ESI) of C<sub>20</sub>H<sub>14</sub>N<sub>2</sub>O<sub>4</sub>SNa [M + Na]<sup>+</sup> calcd, 383.0466; found, 383.0453.

**Biological Assays. Cell Lines.** Human breast cancer cell line (MCF-7), human sarcoma cell lines (RD2, RH30 and U2OS), and human medulloblastoma cell line (DAOY) were maintained in Dulbecco's Modified Eagle Medium (DMEM) supplemented with 10% penicillin/streptomycin FBS and stored in a humidified 37 °C incubator with 5% CO<sub>2</sub>.

**STAT3 Inhibitors.** **8**, **11**, and **13** were dissolved in sterile DMSO to make 20 mM stock solutions. Aliquots of the stock solutions were stored at –20 °C.

**Cell Viability Assay.** Human sarcoma cell lines (RD2, RH30, U2OS) were seeded in 96-well plates at a density of 3000 cells per well. The cells were incubated at 37 °C for a period of 24 h. Different concentrations of **8** (0.1–10  $\mu$ M), **11** (0.1–20  $\mu$ M), and **13** (0.1–10  $\mu$ M) were added in triplicate to the plates in the presence of 10% FBS. 3-(4, 5-Dimethylthiazolyl)-2, 5-diphenyltetrazoliumbromide (MTT) was added to evaluate cell viability. The absorbance was read at 595 nm. IC<sub>50</sub> values were determined using SigmaPlot 9.0 Software (Systat Software, Inc., San Jose, CA).

**Western Blot Analysis.** RH30 cells were treated with **8** (0.25–1  $\mu$ M) or **11** (0.5–2.5  $\mu$ M) or DMSO at 60–80% confluence in the presence of 10% FBS for 24 h. The sarcoma cell line EW8 was treated with **8** (0.5–2.5  $\mu$ M) or DMSO at 60–80% confluence in the presence of 10% FBS for 24 h. MCF-7 cells and DAOY cells were treated with DMSO, 25–50 ng/mL of IL-6, **8** (0.25–1  $\mu$ M), or **11** (0.5–2.5  $\mu$ M), protein expressions of P-STAT3 (Tyr705) and STAT3 were tested. DAOY cells were treated with DMSO, 50 ng/mL of IFN- $\gamma$ , or **8** (1–5  $\mu$ M), protein expressions of P-STAT3 (Tyr705) and STAT3 were tested.

**Western blot procedure:** The cells were harvested and lysed in cold radioimmunoprecipitation assay (RIPA) lysis buffer containing proteasome inhibitor cocktail and phosphatase inhibitor cocktail, and were subjected to SDS-PAGE. Then they were transferred to PVDF membrane. Membranes were probed with primary antibodies (1:1,000) and horseradish peroxidase (HRP)-conjugated secondary antibody (1:10,000) (Cell Signaling Technology, Beverly, MA). Membranes were analyzed using Enhanced Chemiluminescence Plus reagents and scanned with the Storm scanner (Amersham Pharmacia Biotech, Inc., Piscataway, NJ).

**IL-6 Induction of STAT3 Phosphorylation.** MCF-7 breast cancer cells were seeded in 10 cm plates and allowed to adhere overnight. The following day, the cells were serum-starved. The cells were then left untreated or were treated with **8** (0.25–1  $\mu$ M) or **11** (0.5–2.5  $\mu$ M) or DMSO. After 5 h, the untreated and **8** or **11** treated cells were stimulated by IL-6 (25 ng/mL). The cells were harvested after 30 min and analyzed by Western blot. DAOY medulloblastoma cancer cells were seeded in 10 cm plates and allowed to adhere overnight. The following day, the cells were serum-starved. The cells were then left untreated or were treated with **8** (1–5  $\mu$ M) or DMSO. After 2 h, the untreated and **8** treated cells were stimulated by IL-6 (25 ng/mL). The cells were harvested after 30 min and analyzed by Western blot.

**IFN- $\gamma$  Induction of STAT1 Phosphorylation.** DAOY medulloblastoma cancer cells were seeded in 10 cm plates and allowed to adhere overnight. The following day, the cells were serum-starved. The cells were then left untreated or were treated with **8** (1–5  $\mu$ M) or DMSO. After 2 h, the untreated and **8** treated cells were stimulated by IFN- $\gamma$  (50 ng/mL). The cells were harvested after 30 min and analyzed by Western blot.

**Mouse Xenograft Tumor Model.** MDA-MB-231 human breast cancer cells ( $5 \times 10^6$ ) were injected subcutaneously into the flank area of 6-week-old female athymic nude mice which were purchased from Harlan (Indianapolis, IN, USA). After tumor development, mice were divided into two treatment groups consisting of eight tumors per group: DMSO vehicle control, IP injection of **8** (5 mg/kg). The inhibitors were formulated with Cremaphor, DMSO, and 5% dextrose to enhance delivery and limit toxicity encountered with DMSO alone as the mixing base. Tumor growth was determined by measuring length (*L*) and width (*W*) of the tumor every other day with a caliper. The tumor volume was calculated according to the formula: Tumor volume =  $0.5236 \times L \times W^2$ . The treatment lasted for 21 days.

**Fluorescence Polarization (FP) Assay.** FP assay was used to analyze the ability of **8** to inhibit phosphopeptide binding to the STAT3 SH2 domain. STAT3 protein and peptides were provided by Dr. Pui-Kai Li's lab. Screening was performed at approximately 37 °C. STAT3 protein was used at 300 nM. The final concentration of buffer components used for all FP assays was 10 mM HEPES (pH 7.5), 1 mM EDTA, 0.1% Nonidet P-40, 50 mM NaCl, and 20% DMSO. Dithiothreitol was not added. **8** was diluted to a series of concentrations (1–200  $\mu$ M) from a 20 mM stock in DMSO. Proteins were incubated with **8** in Eppendorf tubes at room temperature for 60 min prior addition of the 5-carboxyfluorescein labeled peptides. The final concentration of labeled peptide is 10 nM. The mixtures were transferred to a 384 Well Costar Black plate with each concentration repeated in three wells. The mixtures were equilibrated in the incubator at 37 °C for at least 30 min. The FP readings were measured, and the experiments were repeated three times. Inhibition curves with standard deviation were fitted, and  $K_i$  value was determined accordingly.

## ■ ASSOCIATED CONTENT

### ● Supporting Information

Data pertaining to the  $^1\text{H}$  and  $^{13}\text{C}$  NMR and HPLC chromatograms of key compounds and compound **8** inhibitions on OSM stimulated MCF-7 cell STAT1/3/5 phosphorylations results. This material is available free of charge via the Internet at <http://pubs.acs.org>.

## ■ AUTHOR INFORMATION

### Corresponding Author

\*Phone: 614-247-8786. Fax: 614-292-2435. E-mail: [li.728@osu.edu](mailto:li.728@osu.edu).

### Notes

The authors declare no competing financial interest.

## ■ ACKNOWLEDGMENTS

We are grateful to Dr. Pui-Kai Li and his graduate student, Jonathan P. Etter, for providing the purified STAT3 protein and their assistance in FP assays. We are grateful to Dr. Werner Tjarks for analytic HPLC tests. We thank Ryan E. Pavlovicz and Dr. Xiaohua Zhu for paper editing. We thank the Ohio Supercomputer Center for computing resources. The study is partially funded by the Alex's Lemonade Stand Foundation and NIH/NCI SR21CA133652.

## ■ ABBREVIATIONS USED

HPLC, high performance liquid chromatography; DMSO, dimethyl sulfoxide; HEPES, (4-(2-hydroxyethyl)-1-piperazineethanesulfonic acid); EDTA, ethylenediaminetetraacetic acid; TLC, thin layer chromatography; IL-6, interleukin 6; IFN- $\gamma$ , interferon  $\gamma$

## ■ REFERENCES

- (1) Mandal, P. K.; Gao, F.; Lu, Z.; Ren, Z.; Ramesh, R.; Birtwistle, J. S.; Kaluarachchi, K. K.; Chen, X.; Bast, R. C.; Liao, W. S.; McMurray, J. S. Potent and Selective Phosphopeptide Mimetic Prodrugs Targeted to the Src Homology 2 (SH2) Domain of Signal Transducer and Activator of Transcription 3. *J. Med. Chem.* **2011**, *54*, 3549–3563.
- (2) Mandal, P. K.; Ren, Z. Y.; Chen, X. M.; Xiong, C. Y.; McMurray, J. S. Structure–Affinity Relationships of Glutamine Mimics Incorporated into Phosphopeptides Targeted to the SH2 Domain of Signal Transducer and Activator of Transcription 3. *J. Med. Chem.* **2009**, *52*, 6126–6141.
- (3) Liu, A.; Liu, Y.; Xu, Z.; Yu, W.; Wang, H.; Li, C.; Lin, J. Novel small molecule, XZH-5, inhibits constitutive and interleukin-6-induced STAT3 phosphorylation in human rhabdomyosarcoma cells. *Cancer Sci.* **2011**, *102*, 1381–1387.
- (4) Liu, Y.; Liu, A.; Xu, Z.; Yu, W.; Wang, H.; Li, C.; Lin, J. XZH-5 inhibits STAT3 phosphorylation and causes apoptosis in human hepatocellular carcinoma cells. *Apoptosis* **2011**, *16*, 502–510.
- (5) Song, H.; Wang, R.; Wang, S.; Lin, J.; Stark, G. R. A Low-Molecular-Weight Compound Discovered through Virtual Database Screening Inhibits Stat3 Function in Breast Cancer Cells. *Proc. Natl. Acad. Sci. U. S. A.* **2005**, *102*, 4700–4705.
- (6) Schust, J.; Sperl, B.; Hollis, A.; Mayer, T. U.; Berg, T. Stat3: a small-molecule inhibitor of STAT3 activation and dimerization. *Chem. Biol.* **2006**, *13*, 1235–1242.
- (7) Lin, L.; Hutzen, B.; Li, P.-K.; Ball, S.; Zuo, M.; DeAngelis, S.; Foust, E.; Sobo, M.; Friedman, L.; Bhasin, D.; Cen, L.; Li, C.; Lin, J. A novel small molecule, LLL12, inhibits STAT3 phosphorylation and activities and exhibits potent growth suppressive activity in human cancer cells. *Neoplasia* **2010**, *12*, 39–50.
- (8) Hajduk, P. J.; Greer, J. A decade of fragment-based drug design: strategic advances and lessons learned. *Nature Rev. Drug Discovery* **2007**, *6*, 211–219.
- (9) Chen, Y.; Shoichet, B. K. Molecular docking and ligand specificity in fragment-based inhibitor discovery. *Nature Chem. Biol.* **2009**, *5*, 358–364.
- (10) Lima, L. M.; Barreiro, E. J. Bioisosterism: a useful strategy for molecular modification and drug design. *Curr. Med. Chem.* **2005**, *12*, 23–49.
- (11) Bhasin, D.; Cisek, K.; Pandharkar, T.; Regan, N.; Li, C. L.; Pandit, B.; Lin, J.; Li, P. K. Design, synthesis, and studies of small

molecule STAT3 inhibitors. *Bioorg. Med. Chem. Lett.* **2008**, *18*, 391–395.

(12) Matsuno, K.; Masuda, Y.; Uehara, Y.; Sato, H.; Muroya, A.; Takahashi, O.; Yokotagawa, T.; Furuya, T.; Okawara, T.; Otsuka, M.; Ogo, N.; Ashizawa, T.; Oshita, C.; Tai, S.; Ishii, H.; Akiyama, Y.; Asai, A. Identification of a New Series of STAT3 Inhibitors by Virtual Screening. *ACS Med. Chem. Lett.* **2010**, *1*, 371–375.

(13) Turkson, J.; Kim, J. S.; Zhang, S. M.; Yuan, J.; Huang, M.; Glenn, M.; Haura, E.; Sebt, S.; Hamilton, A. D.; Jove, R. Novel peptidomimetic inhibitors of signal transducer and activator of transcription 3 dimerization and biological activity. *Mol. Cancer Ther.* **2004**, *3*, 261–269.

(14) Ren, X. M.; Duan, L.; He, Q. A.; Zhang, Z.; Zhou, Y.; Wu, D. H.; Pan, J. X.; Pei, D. Q.; Ding, K. Identification of Niclosamide as a New Small-Molecule Inhibitor of the STAT3 Signaling Pathway. *ACS Med. Chem. Lett.* *1*, 454–459.

(15) Siddiquee, K. A. Z.; Gunning, P. T.; Glenn, M.; Katt, W. P.; Zhang, S.; Schroeck, C.; Sebt, S. M.; Jove, R.; Hamilton, A. D.; Turkson, J. An oxazole-based small-molecule Stat3 inhibitor modulates Stat3 stability and processing and induces antitumor cell effects. *ACS Chem. Biol.* **2007**, *2*, 787–798.

(16) Faruqi, T. R.; Gomez, D.; Bustelo, X. R.; Bar-Sagi, D.; Reich, N. C. Rac1 mediates STAT3 activation by autocrine IL-6. *Proc. Natl. Acad. Sci. U. S. A.* **2001**, *98*, 9014–9019.

(17) Yu, H.; Pardoll, D.; Jove, R. STATs in cancer inflammation and immunity: a leading role for STAT3. *Nature Rev. Cancer* **2009**, *9*, 798–809.

(18) Viegas-Junior, C.; Danuello, A.; Bolzani, V. S.; Barreiro, E. J.; Fraga, C. A. M. Molecular hybridization: a useful tool in the design of new drug prototypes. *Curr. Med. Chem.* **2007**, *14*, 1829–1852.

(19) Huey, R.; Morris, G. M.; Olson, A. J.; Goodsell, D. S. A semiempirical free energy force field with charge-based desolvation. *J. Comput. Chem.* **2007**, *28*, 1145–1152.

(20) **2012**: *LigPrep Suite 2012*, version 2.5; Schrödinger, LLC, New York, 2012.

(21) *Schrödinger Suite 2011 Protein Preparation Wizard*; Schrödinger, LLC, New York, 2012; *Epik*, version 2.3; Schrödinger, LLC: New York, 2012; *Impact*, version 5.8; Schrödinger, LLC: New York, 2012; *Prime*, version 3.1; Schrödinger, LLC: New York, 2012.